PLANT SCIENCE

Characterization of a dynamic metabolon producing the defense compound dhurrin in sorghum

Tomas Laursen,[1,2,3,4,5] Jonas Borch,[2,6] Camilla Knudsen,[1,2,3,4] Krutika Bavishi,[1,2,3,4] Federico Torta,[7] Helle Juel Martens,[4] Daniele Silvestro,[4] Nikos S. Hatzakis,[2,8] Markus R. Wenk,[7,9] Timothy R. Dafforn,[10,11] Carl Erik Olsen,[1,2,3] Mohammed Saddik Motawia,[1,2,3,4] Björn Hamberger,[1,2] Birger Lindberg Møller,[1,2,3,4,12]* Jean-Etienne Bassard[1,2,3,4]*

Metabolic highways may be orchestrated by the assembly of sequential enzymes into protein complexes, or metabolons, to facilitate efficient channeling of intermediates and to prevent undesired metabolic cross-talk while maintaining metabolic flexibility. Here we report the isolation of the dynamic metabolon that catalyzes the formation of the cyanogenic glucoside dhurrin, a defense compound produced in sorghum plants. The metabolon was reconstituted in liposomes, which demonstrated the importance of membrane surface charge and the presence of the glucosyltransferase for metabolic channeling. We used in planta fluorescence lifetime imaging microscopy and fluorescence correlation spectroscopy to study functional and structural characteristics of the metabolon. Understanding the regulation of biosynthetic metabolons offers opportunities to optimize synthetic biology approaches for efficient production of high-value products in heterologous hosts.

Plants produce a plethora of specialized metabolites to fend off attack from herbivores and pests and to adapt to abiotic stresses. One class of specialized metabolites is the cyanogenic glucosides, such as dhurrin, which is present in *Sorghum bicolor* (*1*). Dhurrin is produced from the amino acid L-tyrosine and synthesized by three membrane-anchored proteins—the NADPH (reduced nicotinamide adenine dinucleotide phosphate)–dependent cytochrome P450 oxidoreductase (POR) and two cytochrome P450 enzymes (CYP79A1 and CYP71E1)— and by a soluble UDP (uridine diphosphate)–glucosyltransferase (UGT85B1) (*2*) (Fig. 1A). When cellular integrity is disrupted, such as by a chewing insect, dhurrin is hydrolyzed, which results in the release of toxic hydrogen cyanide (Fig. 1A) (*1*).

[1]Plant Biochemistry Laboratory, Department of Plant and Environmental Science, University of Copenhagen, DK-1871 Frederiksberg C, Denmark. [2]bioSYNergy, Center for Synthetic Biology, DK-1871 Frederiksberg C, Denmark. [3]VILLUM Research Center for Plant Plasticity, DK-1871 Frederiksberg C, Denmark. [4]Copenhagen Plant Science Center, University of Copenhagen, DK-1871 Frederiksberg C, Denmark. [5]Feedstocks Division, Joint BioEnergy Institute, Emeryville, CA 94608, USA. [6]VILLUM Center For Bioanalytical Sciences, Department of Biochemistry and Molecular Biology, University of Southern Denmark, DK-5230 Odense M, Denmark. [7]Department of Biochemistry, Yong Loo Lin School of Medicine, National University of Singapore, Singapore 117597, Singapore. [8]Department of Chemistry, Nano-Science Center, University of Copenhagen, DK-2100 Copenhagen, Denmark. [9]Department of Biological Sciences, Yong Loo Lin School of Medicine, National University of Singapore, Singapore 117597, Singapore. [10]School of Biosciences, University of Birmingham, Birmingham B15 2TT, UK. [11]Department of Business, Energy and Industrial Strategy, Her Majesty's Government, UK. [12]Carlsberg Research Laboratory, DK-1799 Copenhagen V, Denmark.
*Corresponding author. Email: blm@plen.ku.dk (B.L.M.); jbassard@outlook.com (J.-E.B.)

The dhurrin content of 3-day-old etiolated seedlings reaches 30% of their dry weight (*3*), even though the enzymes involved in dhurrin biosynthesis constitute less than 1% of the total membrane protein content (*4*). This efficiency may be governed by metabolon formation. Metabolon disassembly would result in the release of an aldoxime intermediate, which has been proposed to act as an antifungal agent (*5*). Several biosynthetic pathways have been proposed to involve the formation of metabolons, which are often depicted as static entities composed of equimolar protein components (*2, 6–8*). Here we report protein-protein interactions (including oligomer formation), protein dynamics, and functional regulation of the metabolon that catalyzes dhurrin synthesis.

The isolation of dynamic membrane-embedded metabolons is hampered by their destabilization and dissociation upon detergent solubilization of the lipid bilayer. The use of the styrene maleic acid (SMA) copolymer circumvents these issues. The SMA polymer spontaneously integrates into the lipid bilayer and carves out discrete lipid particles (SMALPs) containing the resident membrane proteins and the surrounding lipids (*9*). We used the SMALP technology in combination with affinity chromatography to isolate the dynamic dhurrin metabolon (fig. S1).

Application of the SMA polymer to microsomes prepared from etiolated sorghum seedlings resulted in the formation of discrete SMALPs ranging from 10 to 25 nm in diameter (n = 242) (Fig. 1B). These particles were larger than previously reported SMA particles obtained from pure lipids or harboring a single protein (10 nm on average) (*9*). POR is the common electron donor to all microsomal P450s (*10*). The SMALPs were purified by 2′,5′ADP (adenosine diphosphate)–Sepharose affinity chromatography, based on the NADPH cofactor requirement of POR, for copurification of POR-associated proteins (fig. S2). We analyzed the protein content in the course of SMALP purification by quantitative mass spectrometry (Fig. 1C, fig. S3, and data S1 and S2) (*11*). As a control, the same purification was carried out using the anionic detergent cholate instead of the SMA polymer. The protein enrichment was determined on the basis of the content of the three POR isoforms (POR2a to -c), the P450 proteins, and other enzymes including UGT85B1, dhurrinase, cytochrome b_5 ($Cytb_5$), and $Cytb_5$ reductase (table S1). Microsomal and SMA-solubilized fractions had similar protein content (fig. S3). After affinity chromatography, 132 proteins were quantified in the SMALPs, with the P450s CYP79A1 and CYP71E1 among the eight most abundant proteins (Fig. 1C). In contrast, no P450 enrichment was observed in the cholate sample (table S1). The soluble UGT85B1 was identified in all samples but could not be quantified in the purified SMALP sample, most likely because of the extensive washing steps during microsome preparation and affinity chromatography. The strong enrichment of the entire complement of membrane-bound dhurrin pathway enzymes in the affinity-purified SMALPs demonstrates that these enzymes are assembled in a metabolon.

Functional regulation of dhurrin biosynthesis as a response to environmental stresses (*1*) likely involves dynamic assembly and disassembly of the metabolon. Therefore, we studied the effect of UGT85B1 on the channeling of L-tyrosine toward dhurrin by in vitro reconstitution of the dhurrin enzymes in liposomes. Catalytic activities of P450s were determined based on the amounts of aldoxime (CYP79A1-mediated) and cyanohydrin (CYP71E1-mediated) produced after administration of radiolabeled L-tyrosine substrate (Fig. 2A). In the absence of UGT85B1, 50% of the produced aldoxime was further converted into the cyanohydrin, corresponding to a catalytic rate constant for CYP79A1 ($k_{cat}^{CYP79A1}$) of 80 min^{-1} and a $k_{cat}^{CYP71E1}$ of 40 min^{-1}. When supplemented with UGT85B1 in the absence of UDP-glucose, UGT85B1 interacted with the two P450s (fig. S4), increasing their catalytic properties ($k_{cat}^{CYP79A1}$ = 100 min^{-1} and $k_{cat}^{CYP71E1}$ = 80 min^{-1}) and thus demonstrating an increased flux of L-tyrosine through the P450s and improved channeling (80%; Fig. 2A). Addition of UDP-glucose did not further increase the catalytic efficiency of the two P450s or the channeling of the aldoxime. Additionally, UGT85B1 did not stimulate CYP71E1 activity, as observed by administration of aldoxime as a substrate (Fig. 2A). Therefore, we propose that UGT85B1 binds specifically to both P450s and augments the flux and channeling of L-tyrosine toward dhurrin.

The impact of membrane lipid composition on the catalytic activities of the dhurrin pathway P450s was examined by reconstitution experiments in liposomes, using different ratios of phospholipids based on the enrichment observed in the purified SMALP samples (fig. S5 and data S3 to S5). CYP79A1 activity was marginally influenced by the phospholipid composition. In contrast, the

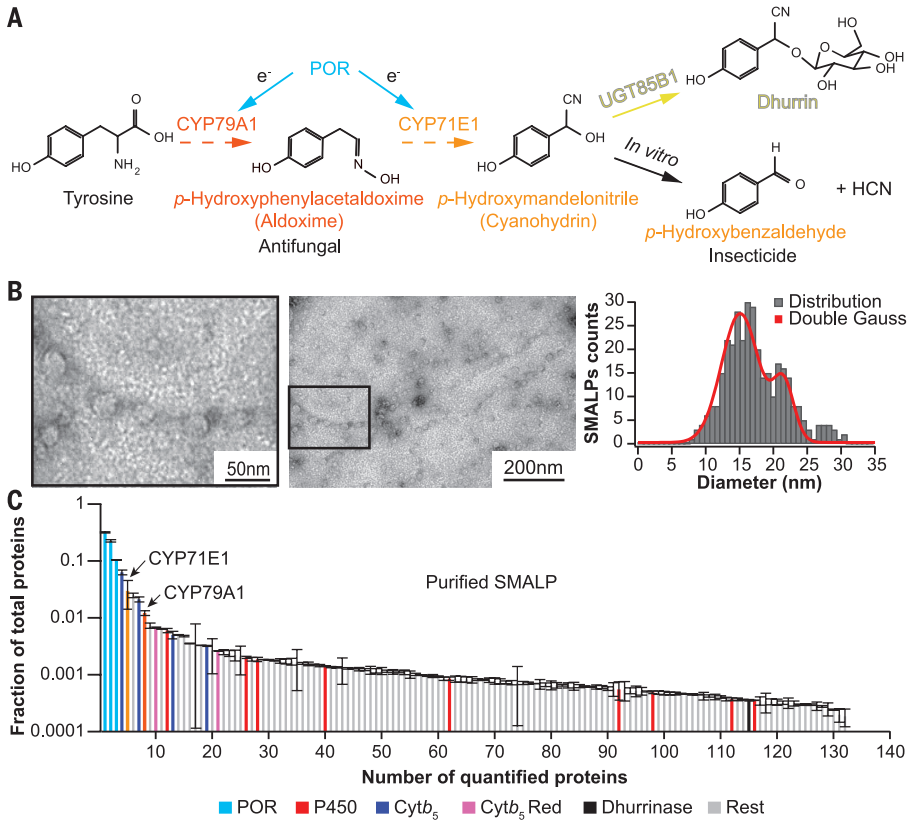

Fig. 1. Detergent-free isolation of the dhurrin metabolon, including the surrounding lipids. (**A**) The dhurrin biosynthetic pathway. HCN, hydrogen cyanide. (**B**) Negative-stain transmission electron microscopy images of affinity-purified SMALPs (left) and the distribution of particle sizes (right). (**C**) Quantitative mass spectrometry of the protein content of affinity-purified SMALPs. Proteins related to dhurrin biosynthesis and other P450 enzymes are highlighted. Data are represented as the fraction of the total protein content (mean values of three independent measurements ± SD). Red, reductase.

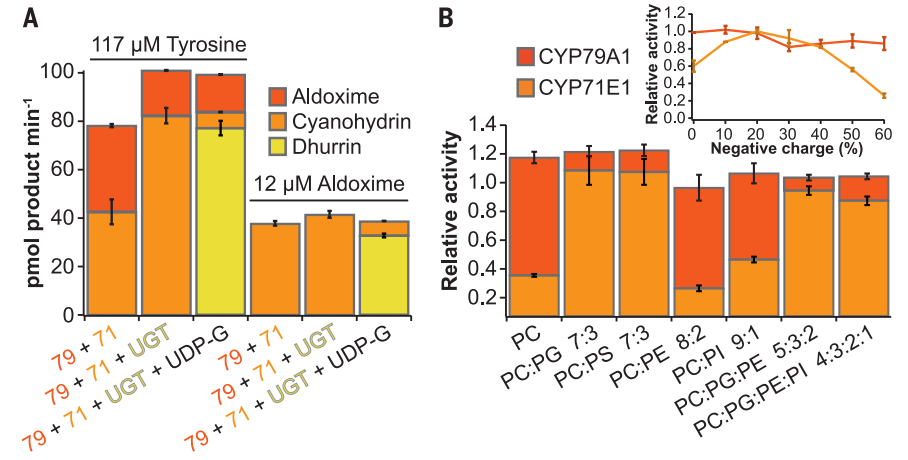

Fig. 2. Protein-protein and protein-lipid interactions stimulate channeling. (**A**) POR2b, CYP79A1, and CYP71E1 were reconstituted in liposomes from a total lipid extract from sorghum microsomes. The catalytic activity of CYP79A1 ("79") and CYP71E1 ("71") was measured in the absence of or after supplementation with UGT85B1 ("UGT") and/or UDP-glucose ("UDP-G"), using radiolabeled L-tyrosine or aldoxime as the substrate. (**B**) POR2b, CYP79A1, and CYP71E1 were reconstituted in liposomes with different lipid mixtures of POPC, POPG, POPS, POPE, and PI. The catalytic activity of CYP79A1 and CYP71E1 was measured and compared with that measured in (A) (relative activity). The inset shows the relative catalytic activity for a titration of PG lipids and P450 activities. All functional data are averages of biological triplicates, and error bars indicate ±SD. PC, 1-palmitoyl-2-oleoyl-*sn*-glycero-3-phosphocholine; PS, 1-palmitoyl-2-oleoyl-*sn*-glycero-3-phospho-L-serine; PG, 1-palmitoyl-2-oleoyl-*sn*-glycero-3-phospho-(1′-rac-glycerol); PI, L-α-phosphatidylinositol; PE, 1-palmitoyl-2-oleoyl-*sn*-glycero-3-phosphoethanolamine.

catalytic efficiency of CYP71E1 was highly sensitive to the lipid environment and dependent on the total concentration of negative charges derived from the lipid headgroups of PG, PS, and PI, with an optimum efficiency in liposomes containing 20 to 30% negatively charged phospholipids (Fig. 2B). This matches the observed enrichment of PG in the purified SMALPs.

To study the organization of the dhurrin pathway enzymes in planta, we transiently expressed CYP79A1, CYP71E1, UGT85B1, POR2b, and different combinations of these (including control proteins) in *Nicotiana benthamiana* leaf epidermal cells (*11*), the most suitable plant expression system for in planta fluorescence lifetime imaging microscopy (FLIM) and fluorescence correlation spectroscopy (FCS). The expression levels of the heterologous proteins in *N. benthamiana* were quantitatively comparable to those in *S. bicolor* seedlings (table S2 and data S6).

Upon coexpression of CYP79A1 and CYP71E1, several byproducts of the dhurrin pathway and some dhurrin accumulated (Fig. 3A). The formation of dhurrin reflects the inherent capability of *N. benthamiana* to glycosylate exogenous compounds (*12*). Coexpression of UGT85B1 with the two P450s and without *S. bicolor* POR2b resulted in the accumulation of 263% more dhurrin and a reduction of byproduct release to 9% of the level observed in the absence of UGT85B1 (table S3). The efficient channeling of intermediates achieved upon coexpression of UGT85B1 supports the assembly of a metabolon in planta and confirms that endogenous *N. benthamiana* POR is sufficient to provide reducing equivalents to the P450s.

To further evaluate dhurrin metabolon formation, we expressed CYP79A1, CYP71E1, UGT85B1, and POR2b as fusion proteins with different fluorescent proteins suitable for in planta FLIM and FCS (figs. S6 to S8) (*11*). First, the functionality of the target enzymes after fusion was assessed. All possible combinations with enhanced green fluorescent protein (eGFP) fused to two of the three target proteins produced similar amounts of dhurrin and byproducts (Fig. 3A and table S3). No apparent difference between the use of N- and C-terminally tagged UGT85B1 was observed, and here we present only the data obtained for N-terminal fusion constructs. The tracking of fluorescent fusion constructs of the dhurrin enzymes with confocal microscopy techniques (movies S1 and S2) illustrated their fast movement in the plant cell along the endoplasmic reticulum (ER) network, as has also been observed in studies of other metabolons (*7*, *8*, *13*). Quantified by FCS, the average diffusion coefficients of individual dhurrin enzymes decreased upon coexpression of the two other partners, whereas the diffusion of the POR2b:eGFP fusion protein was not influenced by coexpression of dhurrin enzymes (Fig. 3, B and C; fig. S9; and tables S4 and S5).

The fluorescence (Förster) resonance energy transfer (FRET) efficiencies from pairwise combinations of all target fluorescent fusion proteins were calculated to gain a more detailed knowledge of the organization of the dhurrin metabolon (fig. S10). The in planta FRET results demonstrated that

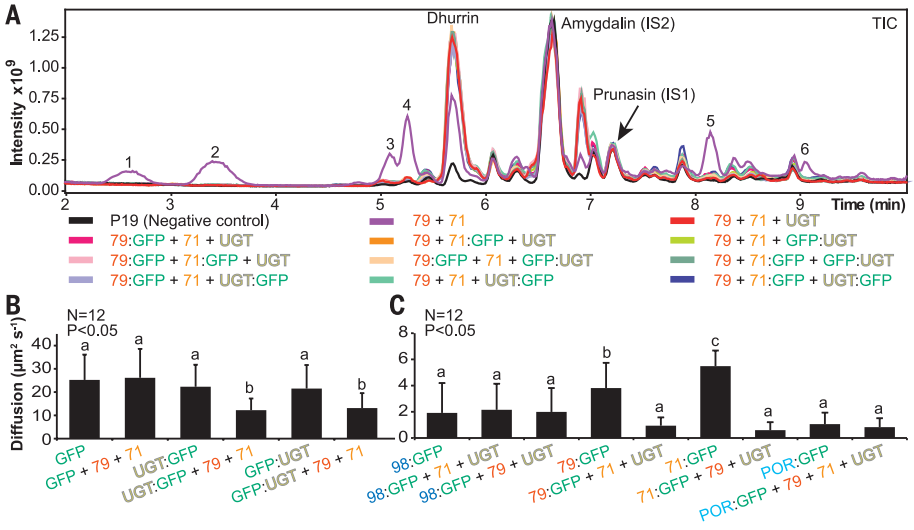

Fig. 3. Functional fluorescence labeling of dhurrin biosynthetic enzymes and control proteins for in planta studies. (**A**) Liquid chromatography–mass spectrometry data for dhurrin biosynthesis in *N. benthamiana* upon expression of CYP79A1, CYP71E1, and UGT85B1. Metabolite profiles were monitored as total ion chromatograms (TICs). Peaks 1 to 6 are byproducts of dhurrin intermediates. Prunasin was used as a primary internal standard and amygdalin as a secondary internal standard. The combination of CYP79A1 and CYP71E1 ("79 + 71") was used as a reference (100%) for the total level of accumulated byproducts. (**B**) Apparent diffusion of eGFP-labeled soluble proteins and (**C**) ER proteins measured by in planta FCS onto ER. CYP98A1:eGFP and free eGFP were used as controls. The CYP98 family of P450 enzymes belongs to the CYP71 clan, like CYP79A1 and CYP71E1. CYP98 catalyzes the introduction of hydroxyl groups at the meta position of phenylpropanoid-derived esters and was chosen as a control because it is not involved in dhurrin metabolism. Letters indicate statistically significant similarities for the recorded values, based on *t* test pairwise comparisons with $P < 0.05$. Error bars indicate ±SD.

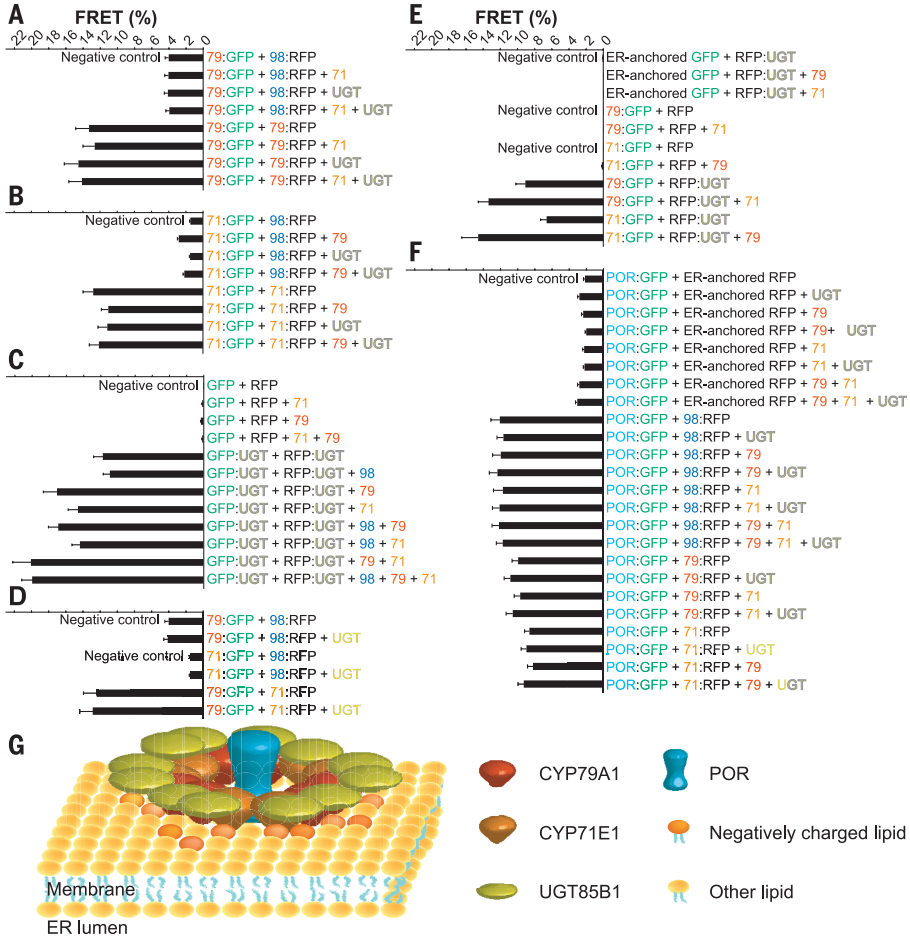

Fig. 4. Protein-protein interactions in planta reveal formation of multienzyme clusters. Pairwise protein association of the dhurrin enzymes was monitored in *N. benthamiana* by FLIM with eGFP- and mRFP1 (monomeric red fluorescent protein 1)–labeled proteins. FRET percentages reflecting the proximity and the frequency of association between protein constructs were calculated from the recorded eGFP lifetime. Error bars indicate ±SD. The effect of coexpression of the third dhurrin enzyme was determined by FRET measurements between the combinations (**A**) CYP79A1-CYP79A1, (**B**) CYP71E1-CYP71E1, (**C**) UGT85B1-UGT85B1, (**D**) CYP79A1-CYP71E1, (**E**) CYP79A1-UGT85B1 and CYP71E1-UGT85B1, and (**F**) POR2b-P450. (**G**) Model of the dhurrin metabolon involving higher-order clusters and enrichment of negatively charged phospholipids.

CYP79A1, CYP71E1, and UGT85B1 all form homo- and hetero-oligomers with FRET values higher than those of the controls (Fig. 4, A to E, and tables S6 to S10). FRET signals for CYP79A1-CYP79A1, CYP71E1-CYP71E1, and CYP79A1-CYP71E1 complexes were unaffected by coexpression of UGT85B1. In contrast, UGT85B1-UGT85B1 oligomerization was enhanced by coexpression of either CYP79A1 or CYP71E1, with the highest FRET signal observed when the entire dhurrin pathway was expressed, suggesting recruitment of UGT85B1 by the P450s (Fig. 4C). We therefore

conclude that the soluble UGT85B1 interacts with both CYP79A1 and CYP71E1, but that it is not necessary for CYP79A1-CYP71E1 complex formation (Fig. 4E). CYP79A1, CYP71E1, CYP98A1, and POR2b are situated very close together at the ER surface and have comparable pairwise FRET values (Fig. 4F and table S11). All microsomal P450s require electron donation from POR; therefore, it is not surprising that CYP98A1 is proximal to the dhurrin biosynthetic enzymes (Fig. 4, A, B, and D). UGT85B1 was situated close to the nonpartner ER membrane proteins, CYP98A1 and POR2b, when CYP79A1 and CYP71E1 were coexpressed (table S12).

A prerequisite to understanding how cells coordinate diverse metabolic activities is to understand how the enzyme systems catalyzing these reactions are organized and their possible enrollment as part of dynamic metabolons. Efforts to maximize product yield from genetically engineered pathways (*14*–*17*) would benefit from this information. In this study, we showed that the dhurrin pathway forms an efficient metabolon. CYP79A1 and CYP71E1 form homo- and hetero-oligomers, which enable recruitment of the cytosolic soluble UGT85B1 (Fig. 4G). UGT85B1 regulates the flux of L-tyrosine and stimulates channeling between CYP79A1 and CYP71E1. Efficient metabolic flux and channeling require an overall negatively charged lipid surface and may provide an additional means for regulating the dynamic assembly necessary to respond swiftly to environmental challenges. A similar organization may characterize the biosynthetic pathways of other specialized metabolites as well.

REFERENCES AND NOTES

1. R. M. Gleadow, B. L. Møller, *Annu. Rev. Plant Biol.* **65**, 155–185 (2014).
2. T. Laursen, B. L. Møller, J. E. Bassard, *Trends Plant Sci.* **20**, 20–32 (2015).
3. B. A. Halkier, B. L. Møller, *Plant Physiol.* **90**, 1552–1559 (1989).
4. O. Sibbesen, B. Koch, B. A. Halkier, B. L. Møller, *Proc. Natl. Acad. Sci. U.S.A.* **91**, 9740–9744 (1994).
5. B. L. Møller, *Science* **330**, 1328–1329 (2010).
6. K. Jørgensen *et al.*, *Curr. Opin. Plant Biol.* **8**, 280–291 (2005).
7. S. An, R. Kumar, E. D. Sheets, S. J. Benkovic, *Science* **320**, 103–106 (2008).
8. K. Mohr, E. Kostenis, *Nat. Chem. Biol.* **7**, 860–861 (2011).
9. S. C. Lee *et al.*, *Nat. Protoc.* **11**, 1149–1162 (2016).
10. T. Laursen *et al.*, *ACS Chem. Biol.* **9**, 630–634 (2014).
11. Materials and methods are available as supplementary materials on *Science* Online.
12. H. M. Ting *et al.*, *New Phytol.* **199**, 352–366 (2013).
13. J. E. Bassard *et al.*, *Plant Cell* **24**, 4465–4482 (2012).
14. I. Wheeldon *et al.*, *Nat. Chem.* **8**, 299–309 (2016).
15. C. Singleton, T. P. Howard, N. Smirnoff, *J. Exp. Bot.* **65**, 1947–1954 (2014).
16. G. Farré *et al.*, *Annu. Rev. Plant Biol.* **65**, 187–223 (2014).
17. J. E. Dueber *et al.*, *Nat. Biotechnol.* **27**, 753–759 (2009).

ACKNOWLEDGMENTS

This research was supported by the VILLUM Research Center for Plant Plasticity; by the bioSYNergy program of Center for Synthetic Biology (University of Copenhagen Excellence Program for Interdisciplinary Research); by a European Research Council Advanced Grant to B.L.M. (ERC-2012-ADG_20120314); and by funding from the VILLUM Foundation Young Investigator Programme to N.S.H. T.L. is recipient of a fellowship awarded by the VILLUM Foundation (project no. 95-300-73023). K.B. was supported by the P4FIFTY Marie Curie Initial Training Network (European Union's 7th Framework Programme). D.S. acknowledges funding from Innovation Fund Denmark (project no. 001-2011-4). F.T. and M.R.W. were supported by grants from the National Research Foundation of Singapore (NRFI2015-05) and a Biomedical Research Council–Science and Engineering Research Council joint grant (112 148 0006) from the Singapore Agency for Science, Technology and Research. T.R.D. acknowledges Biological and Biotechnology Science Research Council grants (BB/J017310/1 and BB/K004441/1). Imaging data were collected at the Center for Advanced Bioimaging, University of Copenhagen. We thank B. A. Halkier, C. Martin, A. Schulz, D. Werck-Reichhart, and anonymous reviewers for critical review of this manuscript. The supplementary materials contain additional data.

SUPPLEMENTARY MATERIALS

www.sciencemag.org/content/354/6314/890/suppl/DC1
Materials and Methods
Figs. S1 to S10
Tables S1 to S14
References (*18*–*30*)
Movies S1 and S2
Data S1 to S6

27 May 2016; accepted 4 October 2016
10.1126/science.aag2347

NEURODEVELOPMENT

The sacral autonomic outflow is sympathetic

I. Espinosa-Medina,[1]* O. Saha,[1]* F. Boismoreau,[1] Z. Chettouh,[1] F. Rossi,[1] W. D. Richardson,[2] J.-F. Brunet[1]†

A kinship between cranial and pelvic visceral nerves of vertebrates has been accepted for a century. Accordingly, sacral preganglionic neurons are considered parasympathetic, as are their targets in the pelvic ganglia that prominently control rectal, bladder, and genital functions. Here, we uncover 15 phenotypic and ontogenetic features that distinguish pre- and postganglionic neurons of the cranial parasympathetic outflow from those of the thoracolumbar sympathetic outflow in mice. By every single one, the sacral outflow is indistinguishable from the thoracolumbar outflow. Thus, the parasympathetic nervous system receives input from cranial nerves exclusively and the sympathetic nervous system from spinal nerves, thoracic to sacral inclusively. This simplified, bipartite architecture offers a new framework to understand pelvic neurophysiology as well as development and evolution of the autonomic nervous system.

The allocation of the sacral autonomic outflow to the parasympathetic division of the visceral nervous system—as the second tier of a "cranio-sacral outflow"—has an ancient origin, yet a simple history: It is rooted in the work of Gaskell (*1*), was formalized by Langley (*2*), and has been universally accepted ever since [as in (*3*)]. The argument derived from several similarities of the sacral outflow with the cranial outflow: (i) anatomical—a target territory less diffuse than that of the thoracolumbar outflow, a separation from it by a gap at limb levels, and a lack of projections to the paravertebral sympathetic chain (*1*); (ii) physiological—an influence on some organs opposite to that of the thoracolumbar outflow (*4*); and (iii) pharmacological—an overall sensitivity to muscarinic antagonists (*2*). However, analysis of cellular phenotype was lacking. Here, we define differential genetic signatures and dependencies for parasympathetic and sympathetic neurons, both pre- and postganglionic. When we reexamine the sacral autonomic outflow of mice in this light, we find that it is better characterized as sympathetic than parasympathetic.

[1]Institut de Biologie de l'École Normale Supérieure (IBENS), INSERM, CNRS, École Normale Supérieure, Paris Sciences et Lettres Research University, Paris, 75005 France. [2]Wolfson Institute for Biomedical Research, University College London, London, UK.
*These authors contributed equally to this work †Corresponding author. Email: jfbrunet@biologie.ens.fr

Cranial parasympathetic preganglionic neurons are born in the "pMNv" progenitor domain of the hindbrain (*5*) that expresses the homeogene *Phox2b* and produces, in addition, branchiomotor neurons (*6*). The postmitotic precursors migrate dorsally (*7*) to form nuclei (such as the dorsal motor nucleus of the vagus nerve) and project through dorsolateral exit points (*7*) in several branches of the cranial nerves to innervate parasympathetic and enteric ganglia. In contrast, thoracic and upper lumbar (hereafter "thoracic") preganglionic neurons, which are sympathetic, are thought to have a common origin with somatic motoneurons (*8*, *9*). By implication, they would be born in the pMN progenitor domain (just dorsal to p3)—thus from progenitors that express the basic helix-loop-helix (bHLH) transcription factor Olig2 (*10*). The sympathetic preganglionic precursors then segregate from somatic motoneurons to form the intermediolateral column in mammals (*11*), project in the ventral roots of spinal nerves together with axons of somatic motoneurons, and, via the white rami communicantes, synapse onto neurons of the paravertebral and prevertebral sympathetic ganglia.

We sought to compare the genetic makeup and dependencies of lower lumbar and sacral (hereafter "sacral") preganglionic neurons with that of cranial (parasympathetic) and thoracic (sympathetic) ones. As representative of cranial preganglionic neurons, we focused on the dorsal motor nucleus of the vagus nerve, a cluster of

Characterization of a dynamic metabolon producing the defense compound dhurrin in sorghum

Tomas Laursen, Jonas Borch, Camilla Knudsen, Krutika Bavishi, Federico Torta, Helle Juel Martens, Daniele Silvestro, Nikos S. Hatzakis, Markus R. Wenk, Timothy R. Dafforn, Carl Erik Olsen, Mohammed Saddik Motawia, Björn Hamberger, Birger Lindberg Møller and Jean-Etienne Bassard

Science **354** (6314), 890-893.
DOI: 10.1126/science.aag2347

Metabolite channeling by a dynamic metabolon

The specialized metabolite dhurrin breaks down into cyanide when plant cell walls have been chewed, deterring insect pests. Laursen *et al.* found that the enzymes that synthesize dhurrin in sorghum assemble as a metabolon in lipid membranes (see the Perspective by Dsatmaichi and Facchini). The dynamic nature of metabolon assembly and disassembly provides dhurrin on an as-needed basis. Membrane-anchored cytochrome P450s cooperated with a soluble glucosyltransferase to channel intermediates toward efficient dhurrin production.

Science, this issue p. 890; see also p. 829